energies

MDPI

Article

Research on Junction Temperature Smooth Control of SiC MOSFET Based on Body Diode Conduction Loss Adjustment

Junke Wu *, Yunpeng Wei, Yuntao Wu, Zhou Wang, Xingyu Li and Xiangnan Wei

School of Mechanical and Electrical Engineering, Guilin University of Electronic Technology, Guilin 541004, China; 20102239@ceic.com (Y.W.); yuntao_wu@mails.guet.edu.cn (Y.W.); wangzhou@mails.guet.edu.cn (Z.W.); xingyu_li@mails.guet.edu.cn (X.L.); weixiangnan@mails.guet.edu.cn (X.W.)
* Correspondence: allenwjk@guet.edu.cn

Abstract: In a converter of actual working condition, the change in the current and voltage of the power device will cause the junction temperature to fluctuate greatly. This device is subjected to high thermal stress due to the change in the junction temperature. Therefore, it is necessary to adopt junction temperature control to reduce or smooth the junction temperature fluctuation, so as to realize the junction temperature control and improve the reliability of the device. At present, the methods for the junction temperature control of power devices have certain limitations and there are few active thermal management methods proposed for SiC device characteristics. In this paper, a method for realizing the smooth control of the junction temperature of a SiC device based on the conduction loss adjustment of the body diode for the SiC device has been proposed, considering that the conduction loss of the body diode is greater than the conduction loss of the SiC MOSFET. The conduction time of SiC MOSFET body diode was adjusted. By adjusting the conduction loss of the SiC MOSFET device, the fluctuation range of the junction temperature of the SiC MOSFET device was controlled, the smooth control of the junction temperature of the SiC device was realized, and the thermal stress of the device was reduced.

Keywords: SiC MOSFET; power semiconductor; junction temperature smoothing control; electric vehicle motor drive inverter; body diode; conduction loss

check for updates

Citation: Wu, J.; Wei, Y.; Wu, Y.; Wang, Z.; Li, X.; Wei, X. Research on Junction Temperature Smooth Control of SiC MOSFET Based on Body Diode Conduction Loss Adjustment. *Energies* **2024**, *17*, 6175. https://doi.org/10.3390/en17236175

Academic Editors: Jingwei Zhang, Jun Zhang, Kun Tan and Hengyu Yu

Received: 7 November 2024
Revised: 28 November 2024
Accepted: 5 December 2024
Published: 7 December 2024

Copyright: © 2024 by the authors. Licensee MDPI, Basel, Switzerland. This article is an open access article distributed under the terms and conditions of the Creative Commons Attribution (CC BY) license (https://creativecommons.org/licenses/by/4.0/).

1. Introduction

Wide band-gap semiconductor materials such as silicon carbide (SiC) and nitride (GaN) have significant advantages in their physical and electrical aspects compared to ordinary silicon (Si) materials. The breakdown electric field strength and band gap of SiC materials are eight times and three times than that of ordinary silicon material [1]. Therefore, SiC material is more suitable for making high-temperature, high-frequency, anti-radiation high-power devices. Power devices made of SiC materials help to improve the efficiency and power density of power electronic systems, and are now widely used in the next generation of high-voltage high-power converters.

SiC MOSFET is the core component of the converter, which plays a decisive role in the safety and reliability of the converter. It is necessary to design a more reliable SiC converter to improve the reliability and prolong the service life of the SiC MOSFET.

The main reason for the failure of power devices is the thermal stress caused by the fluctuation of the junction temperature; the fluctuation of the junction temperature will lead to different degrees of expansion in different layers, resulting in thermal stress impact, which will lead to the fatigue aging of the power devices [2]. The junction temperature fluctuation of the power device is mainly related to the low-frequency junction temperature fluctuation, which is mainly caused by the large-scale random fluctuation of the input and output power of the power converter [3]. The junction temperature of power devices is closely related to their life; according to the device life model studied by LESIT, large temperature fluctuations have a much greater impact on a device's life than small temperature

fluctuations [4,5]. Therefore, it is very necessary for power devices to use effective control methods to achieve junction temperature smoothing control to improve their reliability and prolong their service life [6].

At present, there are several methods for the junction temperature smoothing control of power devices. The first method is the control method based on drive regulation, including the junction temperature control method based on gate current regulation [7], the junction temperature control method based on the three-stage gate drive circuit [8], the junction temperature control method based on the gate resistance network [9], and the junction temperature control method based on the switching frequency [10]. The variable switching frequency may affect the output waveform quality of the converter. For this reason, some scholars have proposed the concept of the life improvement benefit index, which takes into account the adjustable range of the switching frequency and the waveform quality.

The second method is the control method based on the changing modulation strategy, including the junction temperature control method based on space vector pulse width modulation [11] and the junction temperature control method based on hybrid modulation [12]. At present, some scholars have proposed that the finite control set model predictive control in modern control theory can be used to realize the junction temperature control of power devices, and this method has great potential [13]. For this reason, some scholars have proposed multi-parameter optimization through the finite set model's predictive control junction temperature [14,15], changing the device's modulation mode, stabilizing the load current, and reducing the junction temperature fluctuation.

The third method is improving the control method of the buffer circuit, including the method of realizing the junction temperature control based on changing the discharge path of the buffer circuit [16]. In the traditional RCD buffer circuit, an auxiliary switch is added to realize the junction temperature control by changing the discharge path of the buffer circuit. When the auxiliary switch is closed, the buffer capacitor discharges to the power device to increase the loss of the power device. When the auxiliary switch is disconnected, the purpose of reducing the loss of the power device is achieved. When the device is turned on, the peak current flowing through the drain source increases. For this reason, some scholars have pointed out the limitations of this method, and proposed a method of changing the buffer mode to achieve junction temperature control [3]. The conversion of the RC buffer circuit and the RCD buffer circuit is realized by connecting the auxiliary switches. By means of loss compensation, the loss of the power device is kept constant to achieve the purpose of smoothing the junction temperature.

It can be seen from the current research that power device junction temperature control research has achieved a certain adjustment effect, but the control method based on drive adjustment has great limitations, and the design scheme needs to be changed according to different power device models. The method of realizing junction temperature control by changing the modulation strategy to stabilize the load current cannot control the junction temperature of a single power device. The control method of the improved buffer circuit has small limitations and simple control. It can be applied to different power devices and is the optimal choice for current junction temperature smoothing control. However, this method requires an additional circuit, which may reduce the efficiency of the converter. At present, there are few active thermal management methods proposed for SiC device characteristics, and this method does not require additional circuits.

This paper presents a SiC MOSFET junction temperature control method based on lossless buffer switch trajectory adjustment. By changing the conduction time of the SiC MOSFET body diode, the conduction loss of a SiC MOSFET device is adjusted, so as to control the junction temperature of the SiC MOSFET device. The feature of this method is that it does not require an external circuit and can only be applied in converters that require dead time.

2. Conduction Characteristics of SiC MOSFET's Body Diode

Due to the contact between the p-well and the source metal, a pin-type diode structure is formed through the p-well, n-region, and n + substrate. The specific structure of the SiC device is shown in Figure 1 and the equivalent circuit diagram of the SiC device is shown in Figure 2. Therefore, for a bridge topology application in a voltage source conversion circuit, there is essentially a freewheeling diode. The characteristics of this diode correspond to the third quadrant of the I-U characteristic curve of the SiC MOSFET. The manufacturing technology of the SiC MOSFET usually leads to a higher carrier lifetime. Therefore, a higher storage charge and higher diode peak reverse current will be generated in the traditional SiC MOSFET. This is an obstacle for many applications of SiC MOSFET devices. The adjustment of the carrier lifetime can be used to reduce the stored charge, but this must be performed through a separate production step.

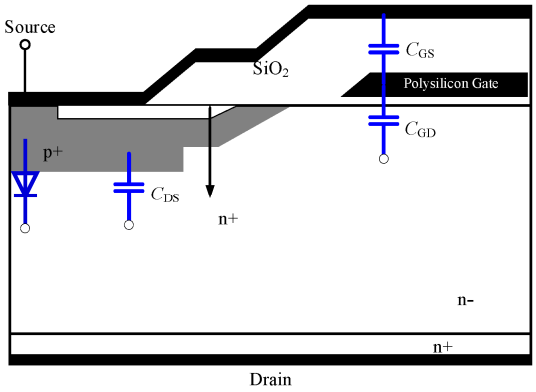


Figure 1. The schematic diagram of a SiC device structure.

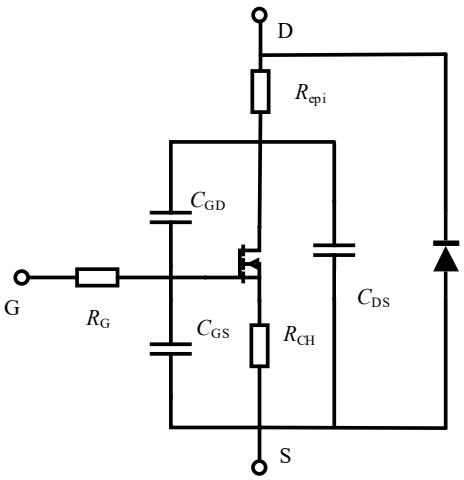


Figure 2. The equivalent circuit diagram of a SiC device.

When the driving voltage at both ends of the gate source is given to −4 V, the body diode of the SiC MOSFET is turned on. At this time, the holes in the P + region and the Pbase region of the SiC MOSFET and the electrons of the substrate will be transported to the N-Drift region due to the applied voltage. At this time, a saddle-like carrier concentration gradient is formed in the N-Drift region, which leads to the weakening of the drift motion, thus generating a diffusion current. The forward current of the bulk diode consists of four parts, namely, the recombination current J_{n-} and J_{n+} generated by the space charge region at the interface of the P + region and the N + region entering the N-Drift region, the electron

diffusion current J_{p+} and J_n entering the P + region and the N-region, and the hole diffusion current J_p entering the N-Drift region. The formula is [17]

$$J = J_{n-} + J_{n+} + J_n + J_{p+} + J_p \tag{1}$$

When a large forward voltage is applied to the SiC MOSFET, the concentration of the non-equilibrium minority carriers injected into the drift region is much larger than the intrinsic carrier concentration. The N-type drift region generates the same concentration of non-equilibrium majority carrier to maintain electrical neutrality, so the hole and electron diffusion currents generate positive currents and the body diode obtains a lower on-state voltage drop. The forward voltage drop of the body diode is composed of the voltage drop of the P + contact region, the voltage drop of the drift region, the PN junction voltage drop composed of the P + region, the N + region, the N-Drift region of the body diode, and the voltage drop of the substrate region. The forward voltage drop of the bulk diode can be expressed as follows:

$$U_F = U_p + U_D + U_{p_{-n^+}} + U_{p_{-n^-}} + U_s \tag{2}$$

In the formula, U_F is the voltage drop when the body diode is turned on. U_{p-n+} and $U_{p\text{-}n\text{-}}$ are the voltage drop of the PN junction formed by the P + region, the N + region, and the N-Drift region of the body diode. U_s is the voltage drop of the substrate region, U_p is the voltage drop of the P + contact region, and U_D is the voltage drop of the drift region.

The resistance of the drift region is related to the conductance modulation effect and the voltage drop of the drift region is affected by the resistance of the drift region. Therefore, the voltage drop of the drift region is mainly analyzed because the conductivity modulation level is related to the carrier lifetime.

$$k_W = \frac{W}{2L_a} \tag{3}$$

In the formula, W is the length of the drift region, and L_a is the diffusion length. The pressure drop in the drift region can be expressed as follows according to the size of k_W:

$$U_D(k_W < 1) = \frac{3kTk_W^2}{q} \tag{4}$$

$$U_D(k_W \geq 1) = \frac{3kT}{8q} e^{k_W} \tag{5}$$

In the formula, q is the elementary charge, T is the absolute temperature, and k is the Boltzmann constant. The diffusion length is determined by the carrier lifetime in the neutral region. The diffusion length can be expressed as follows:

$$L_a = \sqrt{\frac{\mu_n \mu_p}{\mu_n + \mu_p} \tau_H} \tag{6}$$

In the formula, τ_H is the injected carrier lifetime, μ_n is the electron mobility in the bulk diode, and μ_p is the hole mobility in the bulk diode.

3. Junction Temperature Control Based on Body Diode Conduction Loss Adjustment

Since the band gap of the SiC material is three times that of Si material, the PN junction turn-on voltage and forward conduction voltage drop of the SiC MOSFET are higher than those of the Si-based devices, resulting in the conduction loss of the body diode of SiC MOSFET device being greater than the conduction loss during operation. Therefore, the working time of the body diode of the SiC MOSFET affects the loss of the whole chip.

3.1. The Principle of Conduction Loss Adjustment

Figure 3 is the body diode volt–ampere characteristic curve of the Si MOSFET and the SiC MOSFET. In the Figure, the loss of the SiC MOSFET body diode is much larger than that of the Si MOSFET device, and the conduction loss of the SiC device body diode is greater than that of the device conduction. Therefore, the loss of the whole chip can be controlled by controlling the working time of the SiC MOSFET body diode, so as to achieve the purpose of the junction temperature control.

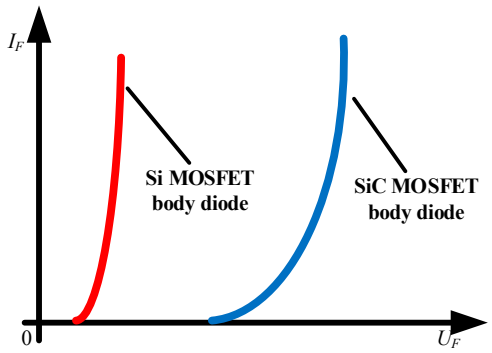


Figure 3. The volt–ampere characteristic curves of body diode of Si and SiC MOSFET.

When the inverter is working, the upper and lower switches of the same bridge arm are forbidden to be connected at the same time in order to avoid a short circuit, and there must be a certain dead time for the upper and lower tube control. During the dead time, when the upper and lower tubes are turned off at the same time, the current flows through the reverse diode of the SiC MOSFET. Due to the large turn-on voltage of the SiC MOSFET body diode, the dead time of the upper and lower tubes can be adjusted; that is, the turn-on time of the SiC MOSFET body diode can be adjusted in a variable direction, so as to realize the adjustment of the conduction loss of the SiC MOSFET, so as to realize the junction temperature equalization control.

The whole commutation process is described by taking the left bridge arm as an example. In Figure 4a, the upper tube is turned on and the lower tube is turned off, and the current flows through the upper tube. In Figure 4b, the upper and lower tubes are turned off at the same time. Since the current direction cannot change abruptly at this time, the current flows through the body diode of the lower tube, resulting in a freewheeling phenomenon. In Figure 4c, the middle and lower tubes are turned on and the upper tube is turned off, and the current flows through the lower tube; the freewheeling process of the upper tube diode in Figure 4d is similar to that in Figure 4b. Based on this principle and these characteristics, a research method based on SiC MOSFET body diode conduction loss adjustment is proposed.

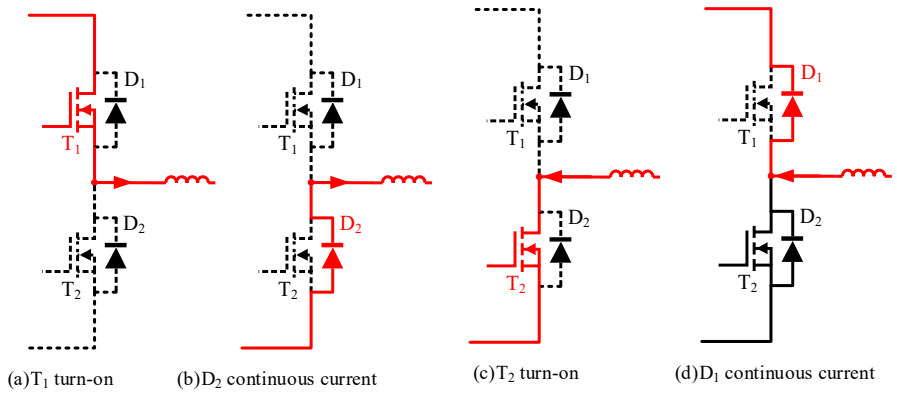


Figure 4. The SiC body diode freewheeling process in the inverter.

3.2. The Influence of Body Diode Conduction Time on the Operation of the Electric Drive Inverter

In the adjustment of the body diode conduction time in the inverter is the adjustment of the dead time of the upper and lower tubes of the same bridge arm. The insertion of the dead time ensures that the switching tubes on the same bridge arm will not be turned on at the same time, which improves the safety of the circuit. However, the dead time will also have some adverse effects on the converter.

When the dead time is set too large, the distortion rate of the PWM waveform will increase, and the output voltage and current of the inverter will produce serious distortion. If the dead time is set too large, it will lead to the distortion of the magnetic chain in the motor control system, which will affect the normal operation of the electric drive inverter. When the dead time is set short, the probability of the switch tube on the same bridge arm of the inverter will increase, which will produce a certain degree of additional power loss, resulting in the heat loss control of the switching device, reducing the physical life of the components in the electric drive inverter, reducing the reliability of the electric drive inverter, and reducing the overall stability and work efficiency of the electric drive inverter control system. Secondly, the dead time also has an effect on the output current of the inverter. When the SVPWM modulation strategy is adopted, if the motor stator current is close to zero in the dead time, the zero current clamping phenomenon will occur due to the addition of the inverter dead time, resulting in the distortion of the current waveform and the fluctuation of the torque. The nonlinear output characteristics of the inverter will affect the stability of the induction motor U/F control system. In addition, the dead time also affects the phase angle of the output voltage. The insertion of dead time leads to an increase in many of the harmonic components in the output waveform of the inverter. The increase in the harmonic components will inevitably lead to the increase in the motor loss, and a large ripple component will be generated in the output torque of the motor, which will cause the oscillation of the motor and the instability of the system.

In the formula, n is the harmonic number, U_{o} is the harmonic voltage, T_{D} is the dead time of the inverter, U_{d} is the pulse voltage, k is the pulse number of half a cycle, and f is the fundamental frequency. According to Formulas (3)–(7), when U_{d}, k, and f are constant, the harmonic content of the output voltage is related to the dead time. The greater the dead time, the greater the harmonic content of the output voltage; the THD (total harmonic distortion) of the output current is also larger [18].

$$\sum_{n=3,5,\ldots}^{\infty} U_o^2 = \frac{1}{\sqrt{2}} \sqrt{\sum_{n=3,5,\ldots}^{\infty} \left(\frac{4kT_D U_d f}{n\pi} \right)^2} \tag{7}$$

Therefore, it is necessary to compensate the dead zone reasonably; as shown in Table 1, setting too long of a dead time will lead to an increase in the THD of the output current and reduce the conversion efficiency of the inverter. In recent years, a variety of effective compensation schemes have been proposed. For example, the hardware circuit is used to detect the pulse width of the switch tube in real time, and is then compared to the command pulse width to obtain the deviation voltage for compensation. However, these measures may not be able to compensate for the impact of nonlinear loads.

Table 1. The influence of the change in dead time on a THD.

Current I_{L}	Dead Time t_{D}	THD
16 A	500 ns	0.15%
16 A	1000 ns	0.30%
16 A	2000 ns	0.60%
16 A	5 μs	1.52%

In general, the influence of dead time on the inverter is mainly reflected in waveform distortion, current distortion, stability reduction, and so on. Therefore, it is necessary to

set the dead time reasonably and take appropriate compensation measures to reduce its adverse effects.

4. Experimental Verification of Body Diode Conduction Adjustment

4.1. The Influence of Body Diode Conduction Time on the Operation of Electric Drive Inverter

The flow chart of active thermal management method for SiC MOSFET devices based on body diode conduction loss adjustment is shown in Figure 5.

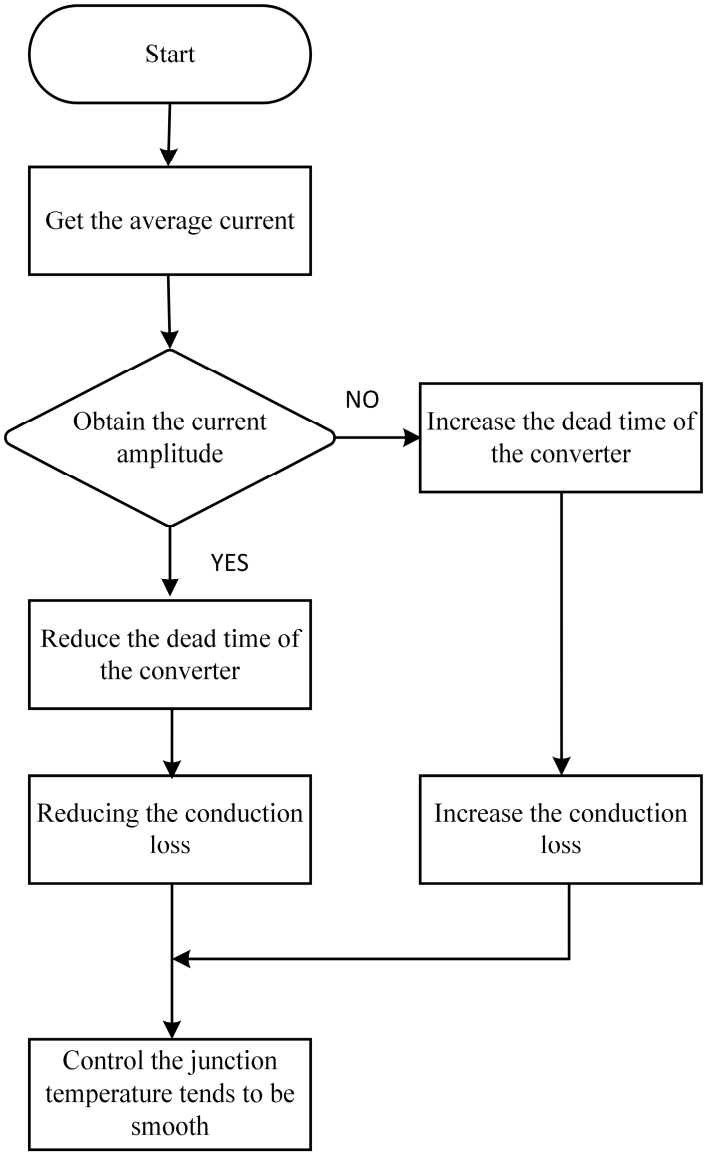


Figure 5. Flowchart of active thermal management of SiC MOSFET.

The experimental verification of body diode conduction loss adjustment is carried out and a simulation verification is carried out on the software Saber. The version number of Saber is 2016. The type number of the SiC MOSFET used in this paper is SCT3030AL, which is produced by Rohm, The Spice model of SiC MOSFET is imported through the device and the inverter simulation platform is built. In the stable operation state, the output current of the inverter load side is 20 A. Table 2 shows the inverter parameters of the simulation design.

Table 2. Inverter simulation parameters.

Symbol	Parameter	Values
U_{dc}	input voltage	200 V
f_m	output frequency	50 Hz
f_w	switching frequency	50 kHz
L_0	load side inductance	1.22 mH
L_{ms}	stray inductance	40 nH

During the simulation process, the load current of 0–0.34 s. 0.68–1 s (*T*1 and *T*3) is maintained at 18 A. The load current of the 0.34–0.68 s (*T*2) cycle is reduced to 16A. At this time, the circuit does not add body diode conduction loss control. In the simulation period of 0–1 s, the inverter dead time is 500 ns. Figure 6 shows the load current and device simulation junction temperature waveform in this state. The upper half of the figure is the load current waveform and the lower half is the device junction temperature waveform of the upper tube of the left bridge arm of the inverter.

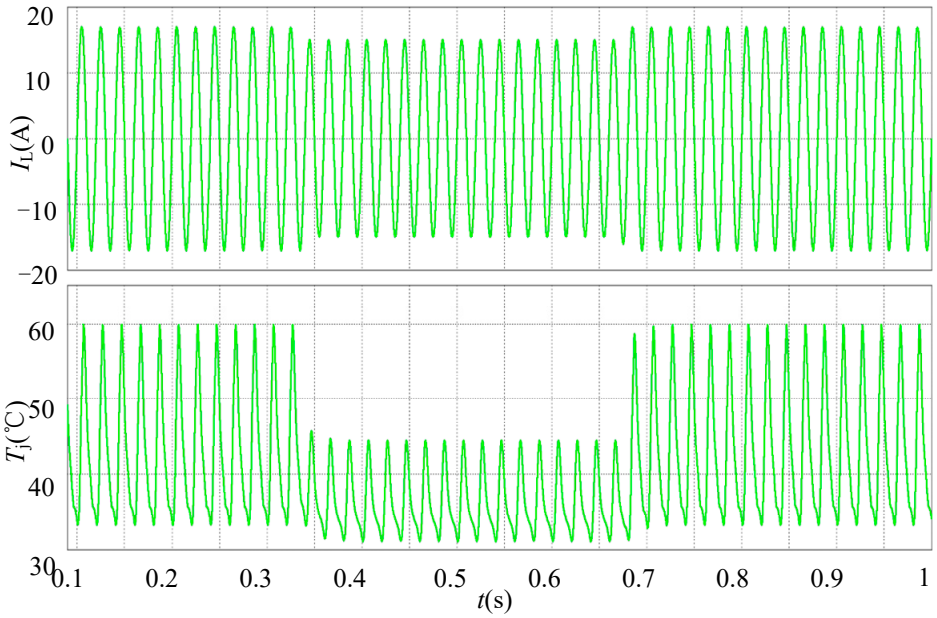


Figure 6. The simulation waveforms of the load current and device junction temperature when the dead time is 500 ns under the inverter commutation.

The body diode conduction loss adjustment is performed for the inverter in this state. In the high current stage (0–0.34 s. 0.68–1 s), the dead time of the converter is reduced to 50 ns to reduce the conduction time of the body diode of the SiC MOSFET device and achieve the purpose of reducing the conduction loss of the SiC MOSFET device. In the small current stage (0.34–0.68 s), the dead time of the converter is increased to 5 µs to increase the conduction time of the body diode of the SiC MOSFET device, so as to increase the conduction loss of the SiC MOSFET device. Table 3 shows the closing parameters of each period before and after the simulation. Under the method of adjusting the conduction loss of the body diode, the change in the junction temperature and the change in the load current are shown in Figure 7. The upper part of the figure is the load current waveform and the lower part is the junction temperature waveform of the device under test.

Table 3. The closing parameters of each period before and after simulation.

Time Interval	Dead Time t_D	Current I_L	THD
Before control T_1 and T_3	500 ns	18 A	0.13%
Before control T_2	500 ns	16 A	0.13%
After control T_1 and T_3	50 ns	18 A	0.01%
After control T_2	5 μs	16 A	1.52%

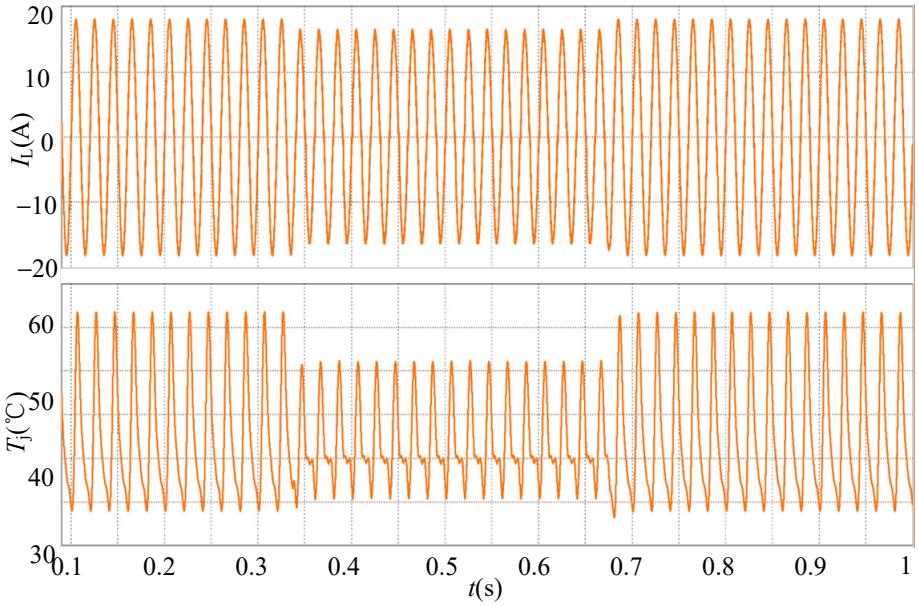


Figure 7. Simulation waveforms of load current and device junction temperature after body diode conduction loss adjustment control.

Due to the lower reduction in the dead time, the junction temperature does not decrease significantly during the small load period. During the large load period, the conduction loss increases due to the increase in the conduction time of the body diode, and the junction temperature of the device increases significantly. However, it can be seen that during the large load period, the load current is distorted. This is exactly what is mentioned in the previous section. The increase in the dead time will lead to the distortion of the load current and the generation of higher harmonics.

Figure 8 shows the waveform comparison before and after the body diode conduction loss control. It can be seen from the figure that after the body diode conduction loss control, when the load current is 18 A, the junction temperature of the device after body diode conduction loss control is slightly lower than that before the body diode conduction loss control in the 0–0.34 s and 0.68–1 s periods. When the load current is 16A, the junction temperature of the device after the body diode conduction loss control is slightly higher than that before the body diode conduction loss control in the period of 0.34–0.68 s. The junction temperature of the device tends to be smooth after control, and the proposed method of the active thermal management of the SiC MOSFET by adjusting the conduction loss of body diode is feasible.

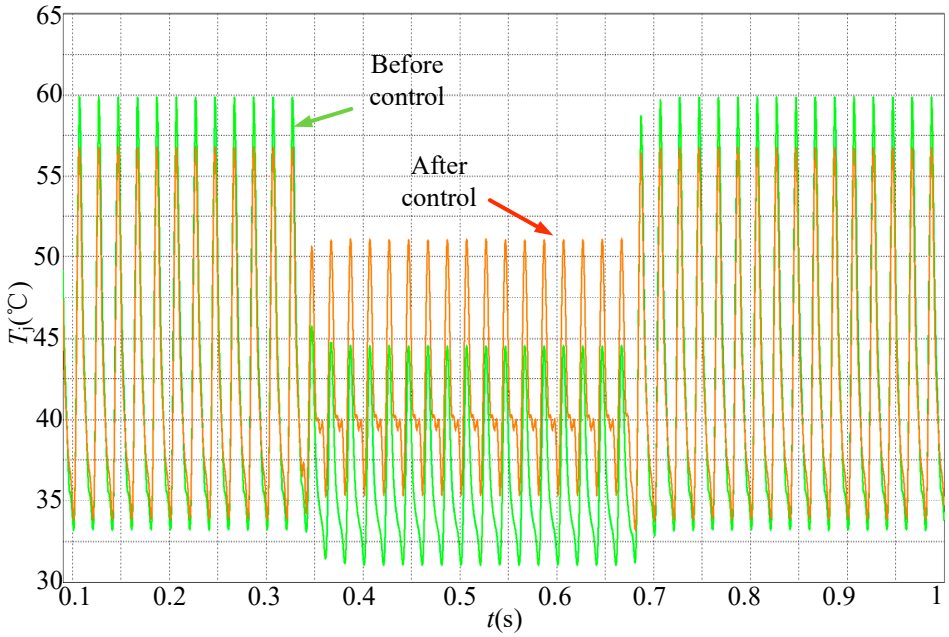


Figure 8. Comparison of device junction temperature simulation waveforms before and after body diode conduction loss adjustment control.

4.2. Experimental Verification Based on Body Diode Conduction Loss Adjustment Method

In order to further study the adjustment method of body diode conduction loss, experiments are carried out on the basis of the simulation platform of Figure 9 to simulate the operating conditions of electric vehicles.

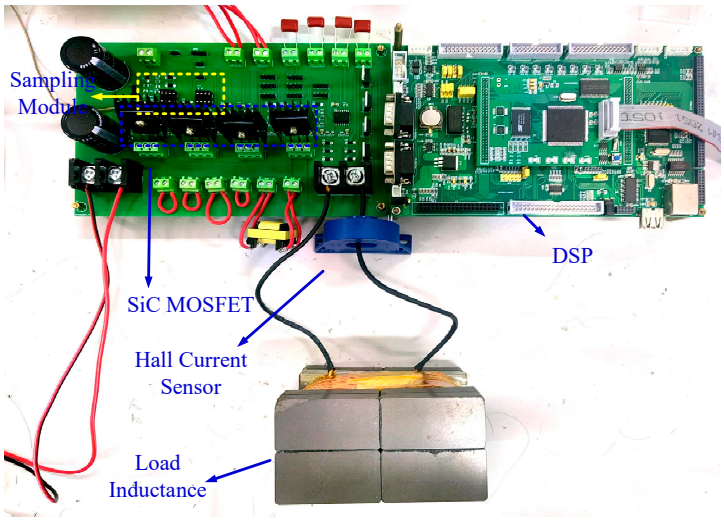


Figure 9. Electric vehicle working condition simulation platform.

The converter control was realized by simulating the operating conditions of the electric vehicles, and the current size was changed every 350 ms. The control current was changed according to the law of 9 A-8 A-9 A and the dead time was 350 ns. Figure 10 shows the load current waveform under the condition of the current change. In this figure, the load current in the large current stage was 9 A, and the load current in the small current stage was 8 A. Under this condition, the junction temperature estimation was carried out, and the junction temperature waveform of the measured device is shown in Figure 11.

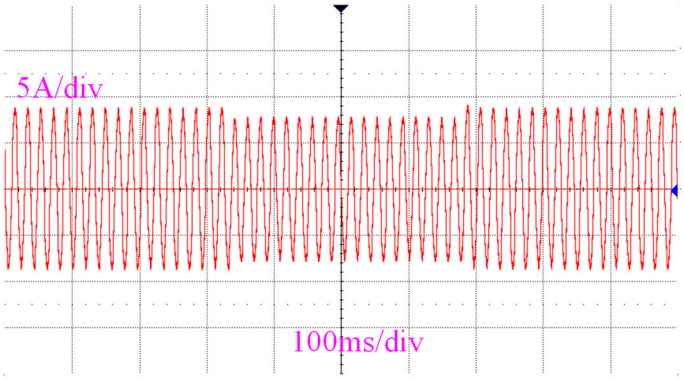


Figure 10. The load current of the experimental platform is 9 A-8 A-9 A.

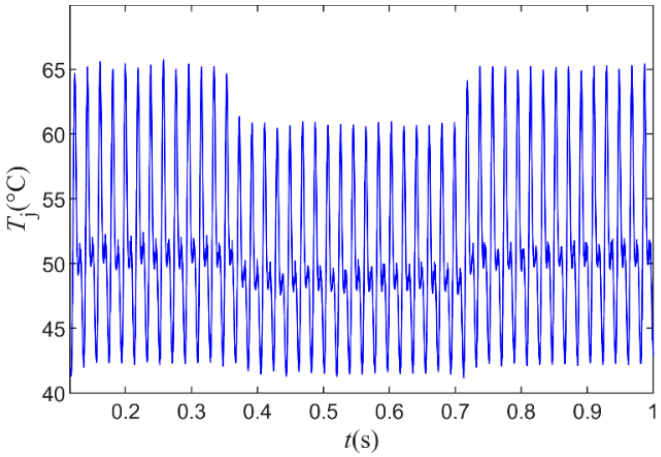


Figure 11. Junction temperature waveform of the device under the test before the conduction loss control of the body diode.

Under the above conditions, the body diode conduction loss control experiment was carried out. In the small current stage, the body diode conduction time of the device under test increased and the dead time was 2 μs. In the large current stage, the body diode conduction time of the device under the test was reduced and the dead time was 100 ns. Table 4 shows the values of the closing parameters in each period before and after the experiment.

Table 4. The closing parameters of each period before and after simulation.

Time Interval	Dead Time t_D	Current I_L
Before control T_1 and T_3	300 ns	9 A
Before control T_2	300 ns	8 A
After control T_1 and T_3	100 ns	9 A
After control T_2	2 μs	8 A

Figure 12 shows the comparison of the waveforms before and after the body diode conduction loss control. The blue waveform in the figure is the junction temperature waveform of the device before the body diode conduction loss control and the pink waveform in the figure is the junction temperature waveform of the device after the body diode conduction loss control. It can be seen from the picture that when the load current is 9 A, the junction temperature of the device is lower than that before the control. When the load current is 8 A, the average junction temperature of the device is similar to that when the load current is 9 A. The junction temperature of the device tends to be smooth after control.

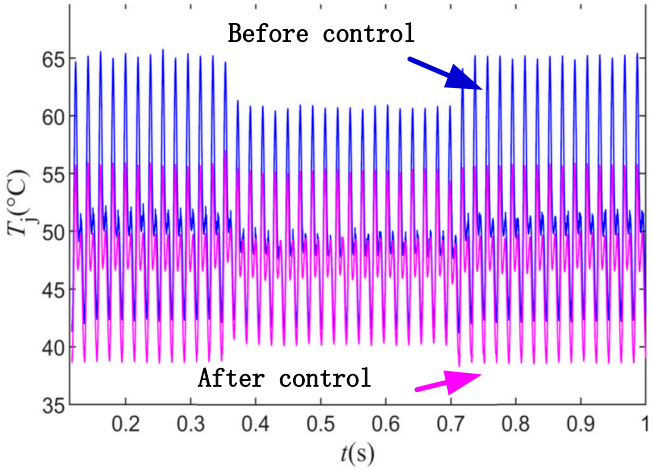


Figure 12. Comparison of the junction temperature waveforms of the device under the test before and after body diode conduction loss control.

After the body diode conduction loss control, the load current was almost unaffected in a certain control range of the dead time, and the load current would not be distorted. Figure 13 shows the load current after the body diode conduction loss control. Figure 13a is the whole current waveform. Figure 13b is the waveform amplified in the high current stage, with an amplitude of 9 A, and Figure 13c is the waveform amplified in the low current stage, with an amplitude of 8 A. It can be seen from Figure 13 that the load current will not be distorted when the dead time does not exceed a certain value.

On the basis of the previous experiment, the dead time of the high current stage is maintained at 100 ns, and the dead time of the low current stage is increased from 2 µs to 3 µs. Table 5 is the value of the shutdown parameters for each period after the experiment.

Table 5. The closing parameters of each period before and after the experiment.

Time Frame	Dead Time t_D	Current I_L
After control (first and third part)	100 ns	9 A
After control (second part)	3 µs	8 A

The load current waveform after the increase in the dead time in the small current stage is shown in Figure 14. Figure 14a is the whole current waveform. Figure 14b is the waveform amplified in the large current stage, and the load current amplitude is 9 A without distortion. Figure 14c is the waveform amplified in the small current stage. The load current amplitude is less than 8 A, and the load current is distorted.

It can be seen from Figure 14 that the dead time is increased to 3 µs in the small current stage, and the load current is distorted from 8 A to below 8 A in the small current stage. Adjusting the dead time can adjust the conduction time of the body diode to change the junction temperature of the device, but too much dead time will lead to distortion of the current which will affect the use of the converter.

4.3. Control Effect Evaluation Based on Body Diode Conduction Loss Adjustment Method

In order to further explore the influence of junction temperature on the life of SiC MOSFET devices, and to evaluate the proposed active thermal management method of SiC MOSFET devices based on body diode conduction loss adjustment, the effect of improving the reliability of the device before and after the control of the on-body diode conduction loss adjustment method was evaluated. The lifetime of the device is closely related to the junction temperature of the device. For the statistics of the junction temperature of the device, the ordinary single-parameter counting method cannot meet the load cycle

characteristics. The method for counting the junction temperature of the power device is generally the rain flow counting method.

The rain flow counting method (tower top method) is widely used to extract the load during the cycle. At first, the rain flow counting method was only considered to be used in material mechanics. The rain-flow counting method can take both the mean value and the fluctuation amplitude into account during the operation. This method divides the whole process into many arithmetical thermal stress fluctuations. In this case, the number of cycles corresponding to each level is drawn, and the fatigue cumulative cycle data are calculated by the number of cycles.

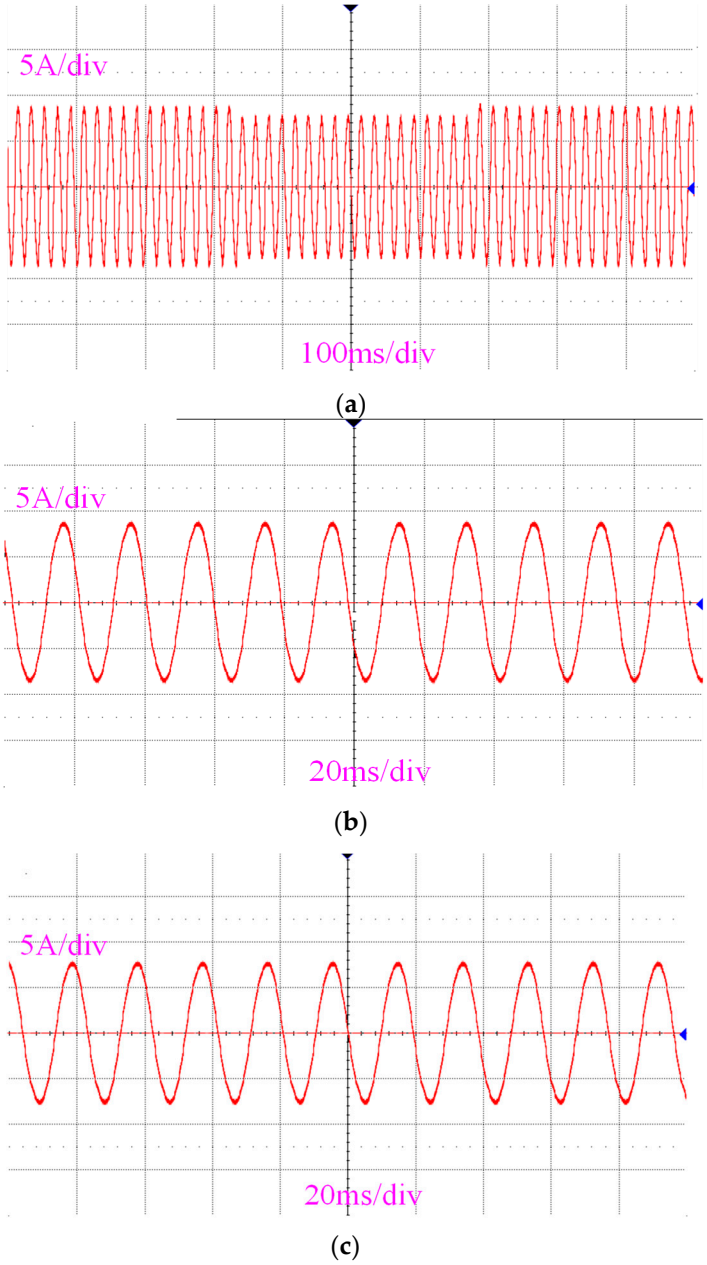


Figure 13. Load current after conduction loss of body diode (dead time of small current is 2 μs). (**a**) The whole current. (**b**) Amplification in high current stage amplification. (**c**) Amplification in the low current stage.

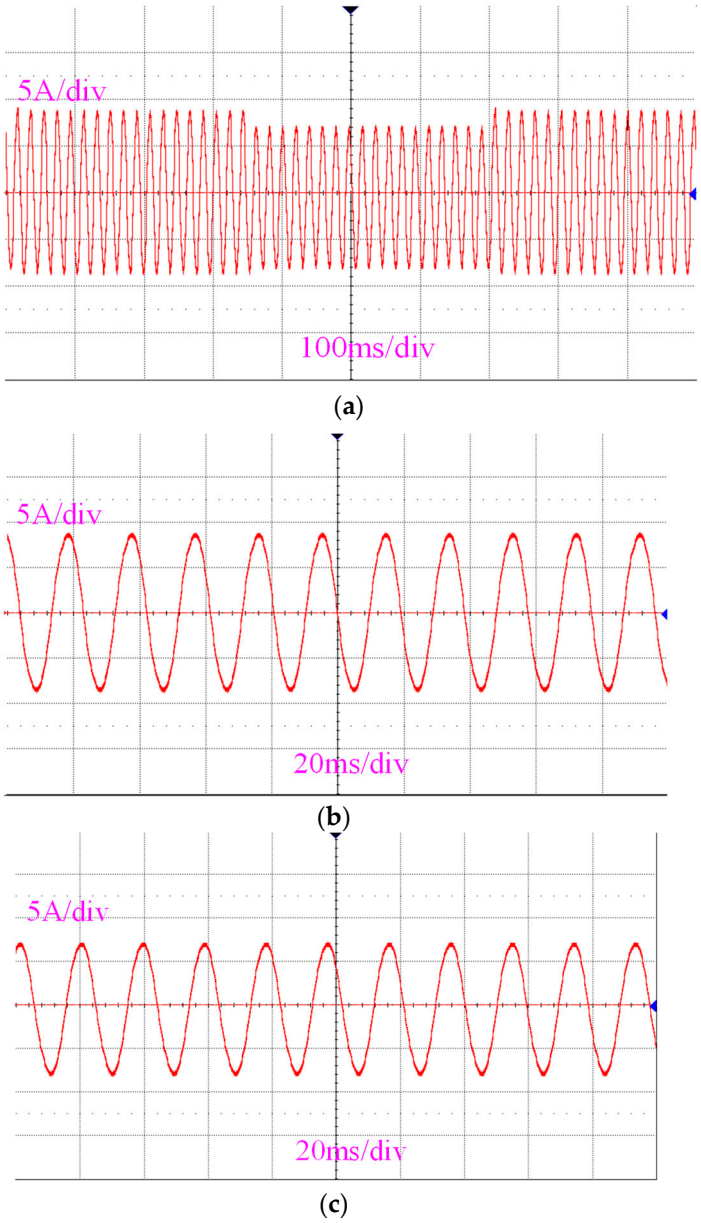


Figure 14. Load current after conduction loss of body diode (dead time of small current is 3 μs). (**a**) Whole current. (**b**) Amplification in large current stage. (**c**) Amplification in low current stage.

Figure 15 shows the heat load histogram of the device under the test before the conduction loss control of the body diode processed by the rain flow counting method. Figure 15 shows the heat load histogram of the device under the test after the conduction loss control of the body diode processed by the rain flow counting method. The main factors affecting the life of a measured power device are the amplitude of the junction temperature change ΔT_j and the average junction temperature $T_{j.m}$. m. The estimation of the number of failed thermal cycles N_f is mainly based on these two parameters. The lifetime of the device is predicted by the junction temperature amplitude, the mean value, and the fluctuation times of each device obtained by the rain flow counting method.

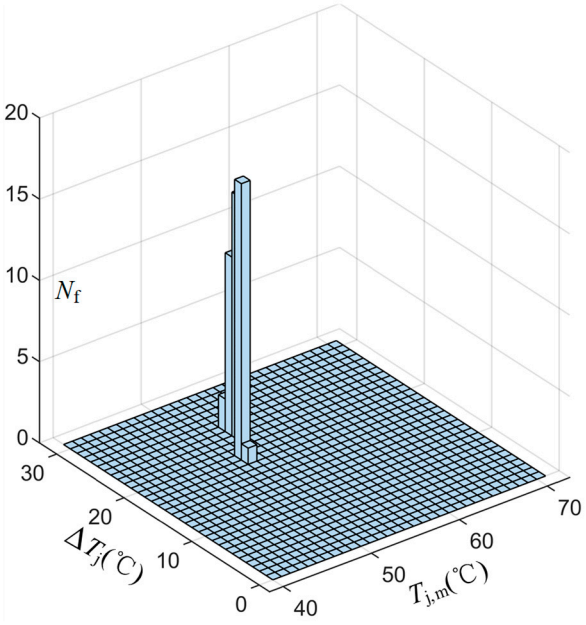


Figure 15. Thermal load histogram of the SiC MOSFET under test before control.

The LESIT model considers the relationship between the number of device failure cycles and the average cycle junction temperature and the amplitude of the cycle junction temperature change. The life prediction model is as follows [4,5]:

$$N_f = A\Delta T_j^{\alpha} e^{\frac{E_\alpha}{k_B(T_{j,m}+273)}} \tag{8}$$

In Formula (8), N_f is the number of device failure cycles. A and α are the experimental coefficients, k_B is the Boltzmann constant, and E_α is the activation energy.

The parameters A and α in Formula (8) are determined according to the power cycle test. In the power cycle experiment, when the time ton15 s of the input stress is applied, the stress is applied to the solder layer. The results of these tests provide data on the reliability of the equipment under the test under specific operating conditions, which is usually provided by the manufacturer. The values of the data are shown in Formula (9) [19].

$$A = 3 \times 10^5, \alpha = -5.039, E_\alpha = 9.98 \times 10^{-20}, k_B = 1.38 \times 10^{-23}. \tag{9}$$

The life estimation is based on Miner's criterion or damage accumulation theory. In practical applications, by correlating the ratio of the number of thermal cycles N_v and the number of relative device failure cycles N_f with ΔT_j and $T_{j.\,m}$, the damage is associated with each stress state. It is assumed that the damage caused by the different temperature fluctuations is independent of each other. So, the total damage Q can be obtained by adding all the damage [20]. Miner's linear fatigue accumulation theorem holds that the damage caused by each cycle is constant regardless of the amplitude of the stress cycle. and these damages can be simply added. This assumption simplifies the prediction process of fatigue life, allowing engineers to easily estimate the life of the material in actual use based on the fatigue performance test results of the material. The linear cumulative damage theory of Palmgren–Miner, called Miner's rule, is reasonable under certain conditions which can simplify the prediction process of fatigue life and give relatively accurate results.

$$Q = \sum_{i=1}^{k} Q_{v,i} = \sum_{i=1}^{k} \frac{N_{v,i}}{N_{f,i}} \tag{10}$$

$$T = \frac{1}{Q} \tag{11}$$

Figure 15 shows the amplitude, fluctuation times, and average value of the junction temperature of a device before the conduction loss control of the body diode can be obtained. Through Figure 16, the amplitude, fluctuation times, and average value of the junction temperature of the device after the body diode conduction loss control can be obtained. By calculating the $Q_{v,i}$ of all the i th operating points of the electric drive inverter, the overall damage of the SiC power device can be predicted. If the damage is less than 1, the power device can withstand the thermal stress in the entire task curve. Otherwise (if the damage is greater than or equal to 1), the equipment is considered to be faulty. T expresses how many cycles the device under the test can cycle before failure occurs. For the 'cycle', the stress input of the rain flow must be considered. Assuming that a cycle corresponds to one second of the steady-state junction temperature, the device life formula can be expressed as follows:

$$Lifetime = \sum_{i=1}^{k} \frac{1}{360 * h\omega Q * 365} \tag{12}$$

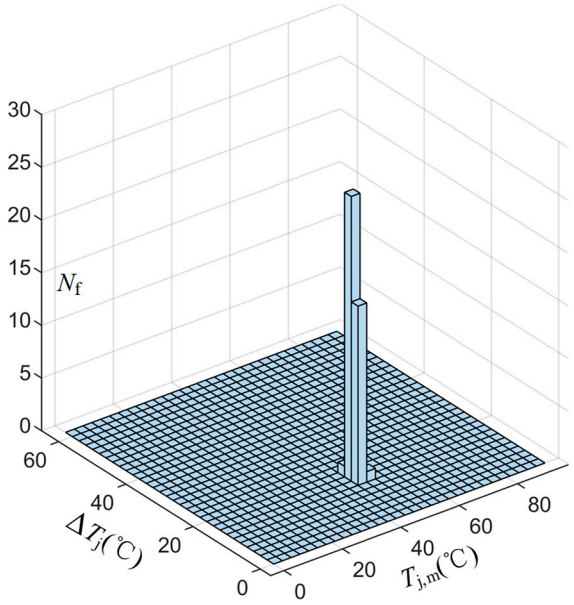


Figure 16. Thermal load histogram of the SiC MOSFET under test after control.

In the formula, ω is the ratio of the i th 'cycle' times to the total 'cycle' times, h is the daily working time of the device, and the value is 24. The Q_A and Q_B of the device before and after the body diode conduction loss control can be obtained by Formulas (8), (10) and (12), and the life of the device before and after the body diode conduction loss control Lifetime_A and Lifetime_B can be obtained by Formula (12).

Table 6 shows the results obtained by using linear fatigue cumulative damage theory and life model. Because the actual working conditions of the electric drive inverter are much more complex than the working conditions listed in this paper, the actual life will be shorter than the life calculated in this paper.

Table 6. Theoretical calculation results of linear fatigue cumulative damage.

	Cumulative Damage	**Device Lifetime**
Before control	1.45×10^{-8}	21.87 years
After control	1.18×10^{-8}	26.87 years

The calculation results of linear fatigue cumulative damage can prove that under the control of body diode conduction loss, the cumulative damage of the device is reduced from 1.45×10^{-8} to 1.18×10^{-8} and the life of the device after junction temperature control

is 1.23 times that before junction temperature control. Experiments show that the proposed method of adjusting the junction temperature of the device through the conduction loss of the body diode can improve the life of the device and improve its operational reliability.

5. Conclusions

Aiming at the method of improving the reliability of SiC MOSFET devices in converters, the method of the smooth junction temperature control of SiC devices based on the adjustment of the body diode conduction loss of SiC MOSFET devices is proposed. The body diode conduction principle of the SiC MOSFET device was analyzed. The feasibility and working principle of adjusting the junction temperature using body diode conduction loss were expounded. The influence of body diode conduction time on a converter was expressed by formula derivation. The correctness of the proposed body diode conduction loss adjustment was further verified using a Saber simulation. Finally, the proposed body diode conduction loss adjustment was verified by experiments. The rain flow counting method and the linear fatigue damage formula were introduced. The life of the device before and after the body diode conduction loss control was evaluated and compared by the rain flow counting method and the linear fatigue damage formula. According to the research methods of this paper, the main conclusions are as follows:

1. Based on the characteristics of SiC MOSFET devices, an active thermal management method based on body diode conduction loss was proposed and the correctness of the proposed method was verified via a simulation and an experiment. Under the comparison of the calculation results of the life prediction model, the conduction loss adjustment of a body diode can effectively extend the life of a SiC device and improve its operational reliability;
2. The control of the body diode conduction time is realized by controlling the dead time of the converter. When the dead time of the converter is too large, it will affect the distortion of the output waveform of the converter.

The method proposed in this paper is based on the conduction loss adjustment of the body diode of the SiC MOSFET device to realize the smooth control of the junction temperature of the SiC device. This method is relatively independent and suitable for most converters. The control method of this method is simple, and the dead time adjustment can be realized by hardware or software.

However, this method is suitable for devices with a large body diode conduction voltage drop; otherwise, the temperature regulation effect is not good. Under actual operating conditions, in order to improve the reliability of the converter, diodes are generally connected in parallel at both ends of the SiC MOSFET device to limit the use of the SiC MOSFET device body diode. The selection of this aspect can be carried out in subsequent research.

Author Contributions: J.W.: conceptualization, methodology, visualization, and writing—original draft. Y.W. (Yunpeng Wei): resources, writing—review and editing, and supervision. Y.W. (Yuntao Wu): software and validation. Z.W.: formal analysis and investigation. X.L.: visualization and writing—review and editing. X.W.: data curation and supervision. All authors have read and agreed to the published version of the manuscript.

Funding: This work was supported by the Innovation Project of GUET Graduate Education (No. 2023YCXS020) and in part by the Guangxi Science and Technology Plan Project under Grant Guike AD20297046.

Data Availability Statement: Data will be made available on request.

Conflicts of Interest: The authors declare no conflicts of interest.

References

1. Minghui, C.; Chunning, W.; Hao, W. Application prospect of SiC power semiconductor devices in modern systems. *Telecom Power Technol.* **2018**, *35*, 11–13.
2. Zhang, J.; Shen, H.; Du, X.; Chen, R. Condition Monitoring the Inhomogeneous Thermal Fatigue of Multichip IGBT Module Based on the Thermal Attenuation Coefficient. *IEEE Trans. Power Electron.* **2025**, *40*, 2114–2125. [CrossRef]
3. Wang, B.; Zhou, L.; Zhang, Y.; Wang, K.; Du, X.; Sun, P. Active Junction Temperature Control of IGBT Based on Adjusting the Turn-off Trajectory. *IEEE Trans. Power Electron.* **2018**, *33*, 5811–5823. [CrossRef]
4. Tang, X.; Zhang, Y.; Sai, Z.; Han, R.; Wu, J.; Pan, Y. Influence of Stray Capacitance on Dynamic Test Results of Power Semiconductor devices. In Proceedings of the 2019 4th IEEE Workshop on the Electronic Grid (eGRID), Xiamen, China, 11–14 November 2019; pp. 1–4.
5. Held, M.; Jacob, P.; Nicoletti, G.; Scacco, P.; Poech, M.H. Fast power cycling test of IGBT modules in traction application. In Proceedings of the Second International Conference on Power Electronics and Drive Systems, Singapore, 26–29 May 1997; Volume 1, pp. 425–430.
6. Wang, X.; Castellazzi, A.; Zanchetta, P. Temperature control for reduced thermal cycling of power devices. In Proceedings of the 2013 15th European Conference on Power Electronics and Applications (EPE), Lille, France, 2–6 September 2013; pp. 1–10.
7. Guo, Y. Study on IGBT Switch Trajectory Adjustment and Junction Temperature Control Based on Active Gate Drive Control. Master's Thesis, South China University of Technology, Guangzhou, China, 2020.
8. Sun, Y.; Sun, L.; Esmaeli, A.; Zhao, K. A Novel Three Stage Drive Circuit for IGBT 2006. In Proceedings of the 1st IEEE Conference on Industrial Electronics and Applications, Singapore, 24–26 May 2006; pp. 1–6.
9. Luo, H.; Iannuzzo, F.; Ma, K.; Blaabjerg, F.; Li, W.; He, X. Active gate driving method for reliability improvement of IGBTs via junction temperature swing reduction. In Proceedings of the 2016 IEEE 7th International Symposium on Power Electronics for Distributed Generation Systems (PEDG), Vancouver, BC, Canada, 27–30 June 2016; pp. 1–7.
10. Falck, J.; Andresen, M.; Liserre, M. Active thermal control of IGBT power electronic converters. In Proceedings of the IECON 2015—41st Annual Conference of the IEEE Industrial Electronics Society, Yokohama, Japan, 9–12 November 2015; pp. 000001–000006.
11. Trzynadlowski, A.M.; Kirlin, R.L.; Legowski, S.F. Space vector PWM technique with minimum switching losses and a variable pulse rate for VSI. *IEEE Trans. Ind. Electron.* **1997**, *44*, 173–181. [CrossRef]
12. Du, X.; Li, G.; Sun, P.; Zhou, L.; Tai, H.M. A hybrid modulation method for lifetime extension of power semiconductors in wind power converters. In Proceedings of the 2015 IEEE Applied Power Electronics Conference and Exposition (APEC), Charlotte, NC, USA, 5–19 March 2015; pp. 2565–2570.
13. Yunhai, W.; Minyou, C.; Wei, L. Review on active thermal control methods based on junction temperature swing smooth control of IGBTs. *Trans. China Electrotech. Soc.* **2022**, *37*, 1415–1430.
14. Ozkan, G.; Papari, B.; Hoang, P.H.; Deb, N.; Edrington, C.S. An Active Thermal Control Method for AC-DC Power Converter with Sequence-based Control Approach. In Proceedings of the 2019 IEEE Electric Ship Technologies Symposium (ESTS), Washington, DC, USA, 14–16 August 2019; pp. 263–267.
15. Falck, J.; Buticchi, G.; Liserre, M. Thermal Stress Based Model Predictive Control of Electric Drives. *IEEE Trans. Ind. Appl.* **2016**, *54*, 1513–1522. [CrossRef]
16. Wu, J.; Zhou, L.; Wang, B. Internal thermal management of power converter based on switching trace adjustment. *J. Power Supply* **2016**, *14*, 46–52.
17. Xie, J. Study on Temperature Characteristics of High Votage SiC MOSFET Body Diode. Master's Thesis, North China Electric Power University, Beijing, China, 2022.
18. Jianfeng, Z. Analysis of the impact of dead-time in inverters on output voltage. *Power Electron.* **2007**, *2*, 792–797.
19. Lai, W.; Chen, M.; Ran, L.; Alatise, O.; Xu, S.; Mawby, P. Low ΔTj Stress Cycle Effect in IGBT Power Module Die-Attach Lifetime Modeling. *IEEE Trans. Power Electron.* **2016**, *31*, 6575–6585. [CrossRef]
20. Wölfle, J.; Röser, T.; Nitzsche, M.; Tröster, N.; Stempfle, M.; Ruthardt, J.; Roth-Stielow, J. Model based temperature control system to increase the expected lifetime of IGBT power modules executed on a neutral point diode clamped three level inverter. In Proceedings of the 2017 19th European Conference on Power Electronics and Applications (EPE'17 ECCE Europe), Warsaw, Poland, 11–14 September 2017; pp. 1–9.

Disclaimer/Publisher's Note: The statements, opinions and data contained in all publications are solely those of the individual author(s) and contributor(s) and not of MDPI and/or the editor(s). MDPI and/or the editor(s) disclaim responsibility for any injury to people or property resulting from any ideas, methods, instructions or products referred to in the content.